ACS OMEGA

Open Access

http://pubs.acs.org/journal/acsodf

Article

Kinetic and Thermodynamic Characteristics of Torrefied *Acer palmatum*

Ailing Lu, Yintao Song,* Dianer Wang, Guangdong Liao, Binguo Zheng, Peng Liu,* and Tingzhou Lei

Cite This: *ACS Omega* 2024, 9, 4474−4485

Read Online

ACCESS | Metrics & More | Article Recommendations

ABSTRACT: The goal of this research was to investigate the effects of torrefying temperature (220, 260, and 300 °C) on the physicochemical properties, kinetics, thermodynamic parameters, and reaction processes of *Acer palmatum* (AP) during the pyrolysis process. The kinetics of raw materials and torrefied biomass were studied by using three kinetic models, and the main function graph approach was employed to find the reaction mechanism. The torrefied biomass produced at temperatures of 220 °C (AP-220), 260 °C (AP-260), and 300 °C (AP-300) was thermogravimetrically analyzed at four different heating rates (5, 10, 15, and 20 °C/min). In comparison to the raw material, the average activation energy of torrefied biomass declined with increasing temperature, from 174.13 to 84.67 kJ/mol (FWO), 172.52 to 81.24 kJ/mol (KAS and DAEM). The volatile contents of AP and AP-220 are higher than those of AP-260 and AP-300, indicating that the random nucleation model occupies the central position. Compared with the raw biomass, the average Gibbs free energy (ΔG) of torrefied biomass increased from 157.97 to 195.38 kJ/mol. The mean enthalpy change (ΔH) during the torrefaction process is positive, while the mean entropy change (ΔS) of the torrefaction of biomass is negative, decreasing from 16.93 to −151.53 kJ/mol (FWO) and from 14.36 to −156.06 kJ/mol (KAS and DAEM). Overall, the findings provide a comprehensive understanding of the kinetics and improved features of torrefied biomass as a high-quality solid fuel.

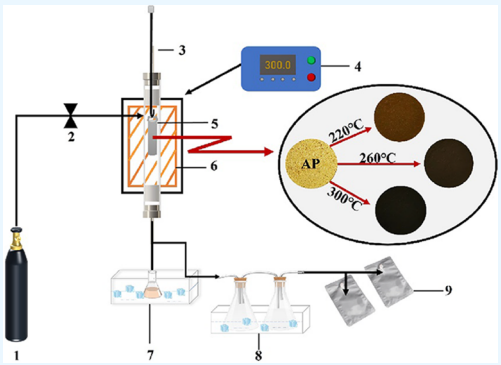

1. INTRODUCTION

With the fast growth of human society and the acceleration of industrialization, greenhouse gas emissions have caused a sustainability dilemma.[1] Although the COVID-19 pandemic had a substantial impact on world health and the economy, climate change may have far more catastrophic implications.[2] Extreme weather events, droughts, floods, and other difficulties caused by climate change might result in food shortages, water scarcity, health challenges, and other human aspects, jeopardizing global society's long-term growth.[3−7] Excessive use of traditional fossil fuels is one of the causes of climate change, which creates environmental issues, notably those connected to carbon dioxide emissions.[8] Energy efficiency and renewable energy sources, such as solar energy, wind energy, geothermal energy, hydropower, and bioenergy, are critical to fulfilling rising energy demands while addressing environmental concerns. Bioenergy, nowadays, is gaining more attention among different renewable energy sources such as solar energy, wind energy, geothermal energy, marine energy, and hydroelectric power.[9] Bioenergy is defined as energy materials derived from organic raw materials such as plants, animals, or microorganisms, such as wood, crop residues, agricultural waste, biomass leftovers, and industrial waste.[10] Bioenergy offers several advantages and disadvantages as a sustainable energy source. To begin with, bioenergy is ecologically beneficial.[11] Bioenergy emits less greenhouse gases such as carbon dioxide during its usage than typical fossil fuels, resulting in less environmental damage.[12] Second, bioenergy has a diverse variety of supplies and may be efficiently utilized through sustainable agriculture and recycling, therefore avoiding energy crises caused by resource depletion.[13] Furthermore, the production and use of bioenergy can stimulate regional economic growth and generate job possibilities.[14] Bioenergy, however, also has significant disadvantages. First, it is challenging to gather, store, transport, and process biomass, and it costs a lot of money and time to do so.[15] Second, different biomass types can create different pollutants during combustion or gasification operations, including exhaust gases, wastewater, and solid waste, having an effect on the environment.[16,17] Additionally, there can be issues with the power density, dependability, and stability of bioenergy. Currently, bioenergy is widely used in several

Received: September 19, 2023
Revised: January 5, 2024
Accepted: January 10, 2024
Published: January 22, 2024

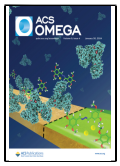

industries, such as transportation, heating, and power generation.[18−21] Biofuels, for instance, may be used to power gas turbines and heat homes. Biomass gasification technology may create synthetic gas and other gases, whereas biomass liquefaction technology can create biodiesel and other fuels. In order to better produce and use bioenergy, many scientists are also investigating strategies to increase the effectiveness of biomass consumption and decrease the environmental impact of bioenergy.

Biomass pyrolysis or torrefaction is an efficient way to transform subpar biomass into high-energy materials with consistent and homogeneous physical and chemical properties in order to enhance the energy and environmental features of biomass for successful energy conversion.[22] Torrefaction is a light thermal treatment that takes place at temperatures between 200 and 300 °C under an environment of regulated oxygen or inert gas for a duration of 30−60 min. Torrefied biomass has better properties than raw biomass, such as a higher heating value and lower hydrogen/carbon (H/C) and oxygen to carbon (O/C) ratios. Additionally, torrefaction makes biomass more easily ground and less likely to absorb water. Torrefied biomass has a greater carbon content and a lower oxygen content than the original biomass, because torrefaction can remove moisture and certain volatile chemicals from the original biomass.

There has already been a substantial amount of research on the kinetic and thermodynamic characteristics of various biomasses.[23−28] The functional link between the pyrolysis kinetics of spruce twigs and rice husks and torrefied temperature was assessed by Bach[29] et al. and Zhang[30] et al., respectively. Three pseudocomponent models were used by Hu[31] et al. to explore the thermal behavior and torrefied kinetics of biomass pellets. Their results showed that the contribution of hemicellulose to the reaction kinetics reduced with an increase in the torrefied temperature because the activation energy of the process dropped. Their results also showed that when the torrefied temperature rises, hemicellulose's contribution to the reaction kinetics declines as a result of the drop in activation energy. Castells[32] and others studied raw palm oil and torrefied palm oil waste samples' combustion kinetic characteristics, and it was discovered that torrefaction increased the activation energy while improving the thermal stability of the samples. Doddapaneni[33] research indicates that the pyrolysis of eucalyptus is somewhat related to its kinetics and reaction mechanism. Bach[34] used independent parallel reaction models for air-torrefaction and kiln-torrefaction to perform a comparative investigation on the thermal deterioration of Norway spruce.

For the design, optimization, and scaling of process reactors and parameters, the kinetic parameters (activation energy and pre-exponential factor), thermodynamic parameters (enthalpy, Gibbs free energy, and entropy), and reaction mechanism are critical.[31] Thermally treated biomass may behave differently than untreated biomass in terms of thermal−chemical conversion. Furthermore, the cofiring of thermally treated biomass with coal in a power plant will be impacted by distinct kinetic, thermodynamic, and reaction processes for both the thermally treated biomass and coal. As a result, a full understanding of the kinetic and thermodynamic parameters as well as the torrefaction biomass reaction process is required. However, it is scarce to systematically express the kinetic and thermodynamic parameters and then illustrate the reaction mechanism of torrefied wood wastes.

The purpose of this research is to investigate the thermal behavior of raw AP and torrefied AP. At different torrefaction temperatures, the thermal breakdown behavior, kinetic parameters, and thermodynamic parameters of raw AP and torrefied sawdust are compared. Proximate analysis, elemental analysis, heating value analysis, and fiber component analysis are used to compare the physicochemical parameters of the original biomass with those of torrefaction biomass. Thermogravimetric methods are used to examine the thermal breakdown behavior and pyrolysis product properties of biomass before and after torrefaction. Flynn−Wall−Ozawa (FWO), Kissinger−Akahira−Sunose (KAS), and distributed activation energy model (DAEM) conversion models are used to determine the kinetic parameters and conduct thermodynamic investigations, providing technical support for thermal−chemical conversion technology from wood waste.

2. MATERIALS AND METHODS

2.1. Material. Lignocellulosic biomasses, AP, from south of Anhui province in China were used as the raw material. They were ground to <0.3 mm and stored under cryogenic environment for subsequent analysis. The proximate analysis was determined by standard method: moisture content (UNE-EN 14774-1:2010), ash content (UNE-EN 14775:2010), volatile matter (UNE-EN 15148:2010), and fixed carbon (determined by mass difference). The elements of C, H, N, and S were monitored using an elemental analyzer (Elementar Vario Micro Cube, Germany), and the percentage of O elements was calculated by mass difference. The heating values of biomasses and biochar were measured with a calorimeter (HYHW-8A, manufactured by He bi Hua yu Instruments LTD), according to GB/T 213-2008. Cellulose, hemicellulose, and lignin contents were determined according to the method proposed by Van Soest.[35] The cellulose content is obtained by treating with acidic detergents, while the hemicellulose content is subtracted from the cellulose content in the residue treated with 72% sulfuric acid. The residue treated with 72% sulfuric acid is dried and then incinerated, and the portion that escapes during the ashing process is the lignin content.

2.2. Torrefaction. The experimental device for the biomass torrefaction process is shown in Figure 1. Torrefaction experiments were carried out in a vertical, 800 mm × 40

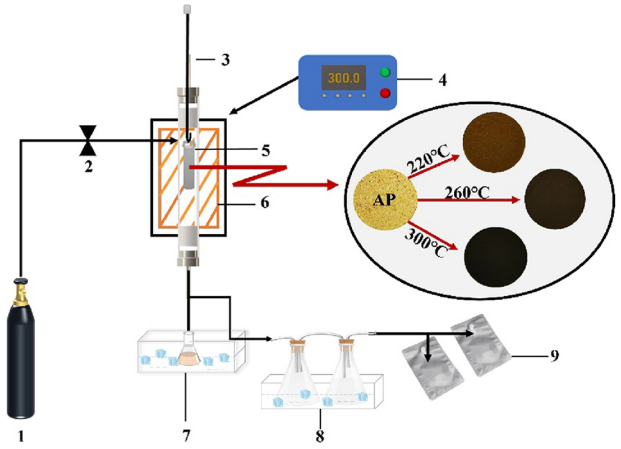

1 Nitrogen Cylinder; 2 Flowmeter; 3 Hanger; 4 Temperature controller; 5 Sample tube; 6 Heating zone; 7 Condensation collection device; 8 Gas-washing bottle; 9 Air bag

Figure 1. Schematic diagram of the experiment.

https://doi.org/10.1021/acsomega.3c07179
ACS Omega 2024, 9, 4474−4485

mm diameter quartz tubular reactor. The samples were placed in the middle 400 mm of the reactor, where isothermal. 10 g of samples was placed in the reactor and heated at 10 °C/min to a set point of 220, 260, and 300 °C for 30 min. Nitrogen with a purity of 99.999% was injected into the reactor at a flow rate of 90 mL/min to create an inert environment and remove the torrefaction gas. After torrefying pretreatment, the reactor was removed from the furnace, and the torrefaction samples were cooled. AP-220, AP-260, and AP-300 represent torrefaction AP at temperatures of 220 °C, 260 °C, and 300 °C, respectively. The basic analyses before and after biomass torrefaction are shown in Table 1.

Table 1. Fundamental Analysis of Raw Biomass and Torrefied Biomass

sample	AP	AP-220	AP-260	AP-300
	Proximate Analysis (%)			
A_d	1.13	1.55	2.90	3.61
V_{daf}	85.12	73.07	46.00	32.03
FC_{daf}	14.88	26.93	54.00	67.97
	Ultimate Analysis (%)			
N[a]	0.39	0.40	0.43	0.55
C[a]	50.53	56.58	70.82	76.75
H[a]	5.95	5.70	4.93	4.42
S[a]	0.00	0.01	0.01	0.01
O[b]	43.12	37.31	23.81	18.27
	Compositional Analysis (%)			
cellulose	44.76	45.46	4.16	0.34
hemicellulose	25.96	5.64	0	0
lignin	17.61	39.81	91.19	96.67
other	11.67	9.09	4.65	2.99
HHV (MJ/kg)	17.98	24.21	30.02	32.47

[a]Nitrogen, carbon, hydrogen, and sulfur elements are measured by elemental analysis instruments. [b]Oxygen element is calculated by difference.

2.3. Thermogravimetric Analysis. A Pyris 1 TGA from PerkinElmer (USA) was used for thermogravimetric analysis to investigate the thermal degradation behavior of AP, AP-220, AP-260, and AP-300. A 15 mg sample was heated from room temperature to 100 °C and held for 1 h to remove moisture. Then, the sample was heated from 100 to 900 °C at heating rates of 5, 10, 15, and 20 °C/min, with a 5 min hold, using 99.999% purity helium (He) as the carrier gas. The data for each thermogravimetric sample were repeated 2−3 times.

2.4. Pyrolysis Kinetics. The typical expression for nonisothermal kinetics of biomass degradation is as follows:

$$\frac{d\alpha}{dt} = kf(\alpha) \tag{1}$$

k is the rate constant; α represents the fractional conversion rate during biomass thermal decomposition.

The biomass conversion rate is defined as

$$\alpha = \frac{(M_0 - M_r)}{(M_0 - M_\infty)} \times 100\% \tag{2}$$

α represents the fractional conversion rate during biomass thermal decomposition; M_0 is the initial mass of the sample, g; M_r is the mass of the sample at any time t, g; M_∞ is the final mass of the sample, g.

The response mechanism is represented by the heterogeneous function $f(\alpha)$, which may be written as

$$f(\alpha) = (1 - \alpha)^n \tag{3}$$

α represents the fractional conversion rate during biomass thermal decomposition; n is the reaction order.

The rate constant varies with the temperature and may be represented as follows:

$$k(T) = A\cdot\exp\left(-\frac{E}{RT}\right) \tag{4}$$

T is the temperature, K; E is the activation energy, kJ/mol; A is the pre-exponential factor, min^{-1}; R is the universal gas constant, 8.314 J/(mol ·K).

Combining eqs 1, 3, and 4 provides the fundamental expression for computing kinetic parameter analysis based on TGA (thermogravimetric analysis) data.

$$\frac{d\alpha}{dt} = A\cdot\exp\left(-\frac{E}{RT}\right)(1 - \alpha)^n \tag{5}$$

α represents the fractional conversion rate during biomass thermal decomposition; n is the reaction order; T is the temperature, K; E is the activation energy, kJ/mol; A is the pre-exponential factor, min^{-1}; R is the universal gas constant, 8.314 J/(mol ·K).

TGA analysis is performed with a constant heating rate; hence, the heating rate is specified as follows:

$$\beta = \frac{dT}{dt} \tag{6}$$

β is the heating rate, K/min.

Temperature influences the conversion rate, although the temperature is also affected by the heating rate. Therefore,

$$\frac{d\alpha}{dT} = \frac{d\alpha}{dt}\frac{dt}{dT} \tag{7}$$

$$\frac{d\alpha}{dT} = \frac{d\alpha}{dt}\frac{1}{\beta} \tag{8}$$

β is the heating rate, K/min.

The rate equation for nonisothermal experiments may be represented as eq 9, by combining eqs 5 and 8:

$$\frac{d\alpha}{dT} = A/\beta\cdot\exp\left(-\frac{E}{RT}\right)f(\alpha) \tag{9}$$

α represents the fractional conversion rate during biomass thermal decomposition; A is the pre-exponential factor, min^{-1}; β is the heating rate, K/min; E is the activation energy, kJ/mol; R is the universal gas constant, 8.314 J/(mol ·K); T is the temperature, K.

We derive the integral function of this by integrating both sides of the equation:

$$g(\alpha) = \int_\alpha^0 \frac{d\alpha}{f(\alpha)} = \frac{A}{\beta}\int_T^0 e^{-E/RT}\,dT \tag{10}$$

$g(\alpha)$ is the integral function of conversion rate α; α represents the fractional conversion rate during biomass thermal decomposition; A is the pre-exponential factor, min^{-1}; β is the heating rate, K/min; E is the activation energy, kJ/mol; R is the universal gas constant, 8.314 J/(mol ·K); T is the temperature, K.

https://doi.org/10.1021/acsomega.3c07179
ACS Omega 2024, 9, 4474−4485

Table 2. Models of Pyrolysis Reactions with Varying $g(\alpha)$ and $f(\alpha)$ Values

reaction mechanism	symbol	$g(\alpha)$	$f(\alpha)$	references
one-dimensional diffusion	D1	α^2	$1/2\alpha$	36
binary diffusion	D2	$(1-\alpha)\ln(1-\alpha) + \alpha$	$[-\ln(1-\alpha)^{-1}]$	28
three-dimensional diffusion	D3	$[1-(1-\alpha)^{1/3}]^2$	$\frac{3}{2}(1-\alpha)^{2/3}[1-(1-\alpha)^{1/3}]^{-1}$	28
three-dimensional diffusion	D4	$1-\frac{2}{3}\alpha-(1-\alpha)^{2/3}$	$\frac{3}{2}[(1-\alpha)^{1/3}-1^{-1}]$	36
geometric contraction	F2	$1-(1-\alpha)^{1/2}$	$2(1-\alpha)^{1/3}$	37
geometric contraction	F3	$1-(1-\alpha)^{1/3}$	$(1-\alpha)^{1/3}$	37
power law	P2/3	$\alpha^{3/2}$	$\frac{2}{3}\alpha^{-1/2}$	37
power law	P2	$\alpha^{1/2}$	$2\alpha^{1/2}$	37
power law	P3	$\alpha^{1/3}$	$3\alpha^{2/3}$	37
power law	P4	$\alpha^{1/4}$	$4\alpha^{3/4}$	36
nucleation and growth	A1	$[-\ln(1-\alpha)]^{2/3}$	$\frac{1}{2}(1-\alpha)[-\ln(1-\alpha)]^{1/3}$	25
nucleation and growth	A2	$[-\ln(1-\alpha)]^{1/2}$	$2(1-\alpha)[-\ln(1-\alpha)]^{1/2}$	25
nucleation and growth	A3	$[-\ln(1-\alpha)]^{1/3}$	$3(1-\alpha)[-\ln(1-\alpha)]^{2/3}$	25
nucleation and growth	A4	$[-\ln(1-\alpha)]^{1/4}$	$4(1-\alpha)[-\ln(1-\alpha)]^{3/4}$	25
first-order random nucleation on a single particle	R1	$-\ln(1-\alpha)$	$(1-\alpha)$	38
second-order random nucleation with two nuclei on a single particle	R2	$(1-\alpha)^{-1}-1$	$(1-\alpha)^2$	38
third-order random nucleation with three nuclei on a single particle	R3	$\frac{1}{2}[(1-\alpha)^2-1]$	$(1-\alpha)^3$	38

The kinetic model $f(\alpha)$ is an algebraic expression that is related to a physical model describing the reaction kinetics. The functions $f(\alpha)$ and $g(\alpha)$ represent different forms of reaction mechanisms, as shown in Table 2.

The thermal breakdown of biomass is a complicated process. As a result, analogous conversion models and distributed models are frequently used to investigate the thermal degradation process in depth. Two common integral approaches for comparable conversion rate modeling are KAS (Kissinger−Akahira−Sunose) and FWO (Flynn−Wall−Ozawa). The distribution of activation energy and pre-exponential factor may be calculated using the equivalent conversion rate approach, which can offer a range for the distributed activation energy and optimize the kinetic parameters.[39]

2.4.1. FWO Model. The FWO model, model free method, provides a more precise way for determining activation energy.[40] $\ln(\beta)$ has a linear connection with $1/T$ at different heating rates. The FWO model may be represented in its simplest form as follows:

$$\ln(\beta) = -1.052\frac{E}{RT} + \ln\left(\frac{AE}{RG(\alpha)}\right) - 5.33 \tag{11}$$

2.4.2. KAS Model. For the KAS model, the linear connection between $\ln(\beta/T^2)$ and $1/T$ at varying heating rates yields the slope E/R, which may be used to calculate the activation energy and frequency factor.[41] The simple KAS model may be written as

$$\ln\left(\frac{\beta}{T^2}\right) = -\frac{E}{RT} + \ln\left(\frac{AE}{RG(\alpha)}\right) \tag{12}$$

2.4.3. Distributed Activation Energy Model (DAEM). DAEM is a useful tool for investigating the response behavior of complicated systems, including an endless number of simultaneous first-order reactions.[39] The process of biomass pyrolysis is described in this work using DAEM. The simplified DAEM model is as follows:

$$\ln\left(\frac{\beta}{T^2}\right) = -\frac{E}{RT} + \ln\left(\frac{AR}{E}\right) + 0.6075 \tag{13}$$

2.4.4. Prediction of Reaction Models. Combination of Criado and main function diagram methods:[36]

$$\frac{Z(\alpha)}{Z(0.5)} = \frac{f(\alpha)\times g(\alpha)}{f(0.5)\times g(0.5)} = \left(\frac{T_\alpha}{T_{0.5}}\right)^2 \times \frac{(\mathrm{d}\alpha/\mathrm{d}t)_\alpha}{(\mathrm{d}\alpha/\mathrm{d}t)_{0.5}} \tag{14}$$

A theoretical curve can be shown in the equation: $\frac{f(\alpha)\times g(\alpha)}{f(0.5)\times g(0.5)}$ to reflect the properties of various reaction processes $\left(\frac{T_\alpha}{T_{0.5}}\right)^2 \times \frac{(d\alpha/dt)_\alpha}{(d\alpha/dt)_{0.5}}$ is the experimental curve derived from experimental values. Using $\alpha = 0.5$ as the reference value, the principal curves of all reaction mechanisms cross the experimental curve at $Z(\alpha)/Z(0.5) = 1$. The major reaction mechanism of the experimental values may be established by comparing the theoretical curve to the experimental curve. As the reaction mechanism,[37] the theoretical curve that is closest to the observed curve is chosen.

2.5. Thermodynamic Analysis. The thermodynamic parameters can be used for estimating the feasibility of combustion, which includes enthalpy (ΔH), Gibbs free energy (ΔG), and entropy (ΔS). These parameters can be evaluated depending on the following equations:

$$\Delta H = E + RT\ln\left(\frac{k_B T}{hA}\right) \tag{15}$$

$$\Delta G = E + RT \tag{16}$$

$$\Delta S = \frac{\Delta H - \Delta G}{T} \tag{17}$$

where ΔG is the Gibbs free energy, kJ/mol; ΔH is the enthalpy change, kJ/mol; ΔS is the entropy change, J/(mol·K); k_B is the Boltzmann constant, 1.38×10^{-23} J/K; h is the Planck constant, 6.626×10^{-34} J s.

https://doi.org/10.1021/acsomega.3c07179
ACS Omega 2024, 9, 4474−4485

3. RESULTS AND DISCUSSION

3.1. The Physicochemical Parameters of AP Prior to and after Torrefaction. The industrial, elemental, fiber content, and heating value of raw (AP) and torrefied biomass (AP-220, AP-260, and AP-300) are shown in Table 1. The results show that when the torrefaction temperature rises, the fixed carbon and ash contents rise from 14.88% to 67.97% and 1.13% to 3.61%, respectively. The elimination of water and volatile materials at high temperatures results in an increase in the fixed carbon content of torrefied biomass. Furthermore, at lower temperatures (220 °C), cellulose breakdown is minimal, resulting in a larger solid yield. However, at higher temperatures (300 °C), hemicellulose decomposes with cellulose and lignin, reducing the hemicellulose and cellulose contents from 25.96% to 0% and 44.76% to 0.34%, respectively, resulting in a loss in solid yield. Because hemicellulose decomposes at lower pyrolysis temperatures, biomass with a greater hemicellulose content produces less solid products during the torrefaction process than liquid and gas products.[42] Furthermore, at higher temperatures, the breakdown of hydroxyl groups accelerates, resulting in more volatile molecules. The qualities of the torrefied products are also determined by the content of the biomass. As illustrated in Figure 2, as the torrefaction temperature rises from 220 to 300 °C, the H/C ratio falls by 0.69, and the O/C ratio falls by 0.64. The elimination of hydrogen and oxygen during torrefaction is greater than that of carbon. As a result, both the H/C and O/C ratios fall dramatically. Furthermore, increased carbon content and fixed carbon content due to torrefaction are the causes for the torrefied biomass having a higher heating value than raw biomass. The heating value of the original biomass increases from 17.98 to 32.47 MJ/kg when the torrefaction temperature rises. Coal has a heating value that ranges between 25 and 35 MJ/kg.[43] Torrefied biomass may therefore be compared to lignite and cofired with coal in power plants to generate electricity.

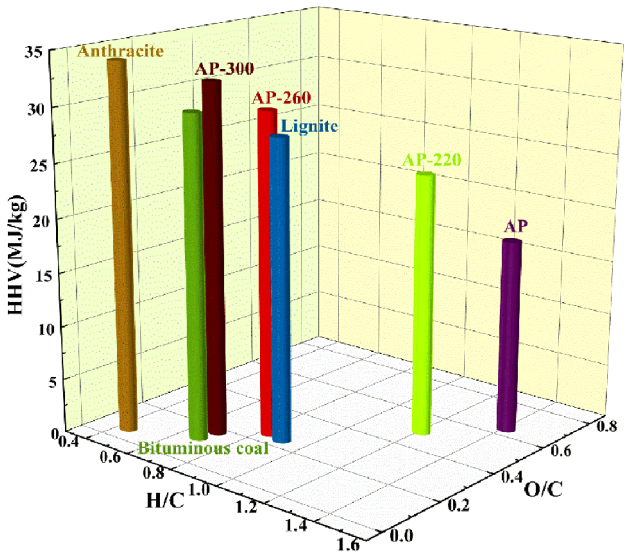

Figure 2. Effect of torrefying temperature on the H/C and O/C ratios and calorific value.

3.2. Thermogravimetric Analysis. Figure 3a–d depicts the pyrolysis behavior of raw biomass and torrefied biomass (AP-220, AP-260, and AP-300) at heating rates of 5, 10, 15, and 20 °C/min. The degradation process is separated into three stages: (1) drying, (2) devolatilization, and (3) char production. The first stage includes the removal of surface moisture as well as certain volatile chemicals.[44] It is also worth noting that the moisture-induced mass loss in torrefied biomass (AP-220, AP-260, and AP-300) is somewhat lower than that in raw biomass. The second stage is connected with devolatilization, which causes considerable mass loss, owing to hemicellulose and cellulose breakdown. The third stage is a sluggish process, caused mostly by char oxidation. Polysaccharides hemicellulose and cellulose have low thermal stability at high temperatures. Lignin, on the other hand, is made up of optically active polymers and has high thermal stability. Temperature ranges for hemicellulose, cellulose, and lignin breakdown are 220−315 °C, 314−400 °C, and 160−900 °C, respectively. It is difficult to identify hemicellulose degradation in the DTG curves of torrefied samples, demonstrating the considerable disintegration of hemicellulose during torrefaction. The major peak in the 300−600 °C range relates mostly to cellulose decomposition,[45,46] with a higher peak intensity seen for AP-220 compared to AP, showing a loss in cellulose thermal stability during moderate torrefaction. The peak intensity related to cellulose is drastically decreased for AP-300 due to severe torrefaction. The peak intensity of cellulose breakdown increases and decreases for mild and severe torrefaction, respectively, compared to raw biomass. Furthermore, when the torrefaction temperature rises, the temperature range for lignin breakdown for AP-260 expands, most likely due to a reduction in the polysaccharide concentration and partial carbonization of sugars.

The DTG curve shows that when the heating rate increases from 5 °C/min to 20 °C/min, the peak of the DTG curve changes slightly toward higher temperatures. This is because the pyrolysis process has a reduced heat transfer efficiency at higher heating rates.[47] Lower heating rates have been found in studies to improve the heat transmission efficiency of biomass particles, resulting in a more uniform pyrolysis breakdown. The greater form of the peak at high heating rates may be ascribed to the compositional variety and complexity of the biomass.[48]

3.3. Kinetic Analysis. The least amount of energy needed for a reaction to take place is called the activation energy. Greater temperatures or longer residence durations are therefore necessary for reactions with higher activation energies in order to generate enough energy for the reaction to proceed. The FWO, KAS, and DAEM methods were used to determine the activation energy for raw biomass and torrefied biomass (AP-220, AP-260, and AP-300), the results are shown in Table 3, which ranged from 146.32 to 187.18 kJ/mol, 171.09 to 205.33 kJ/mol, 60.36 to 134.34 kJ/mol, and 75.75 to 91.08 kJ/mol, respectively. The hemicellulose, cellulose, and lignin components of biomass all have different activation energies. According to Vamvuka[49] et al., cellulose, hemicellulose, and lignin each have an activation energy of 145−285 kJ/mol, 90−125 kJ/mol, and 30−39 kJ/mol, respectively. The largest activation energy is said to be found in cellulose, followed by hemicellulose and lignin. A biomass that has more cellulose will, therefore, have a higher activation energy. According to the table, AP-220 has a little greater relative cellulose content than raw biomass. As a result, AP-220 has a greater activation energy than raw biomass. The breakdown of cellulose becomes considerable as the torrefaction temperature rises. As a result, AP-260 and AP-300 have lower activation energies than raw biomass. AP-300's lower activation energy

https://doi.org/10.1021/acsomega.3c07179
ACS Omega 2024, 9, 4474−4485

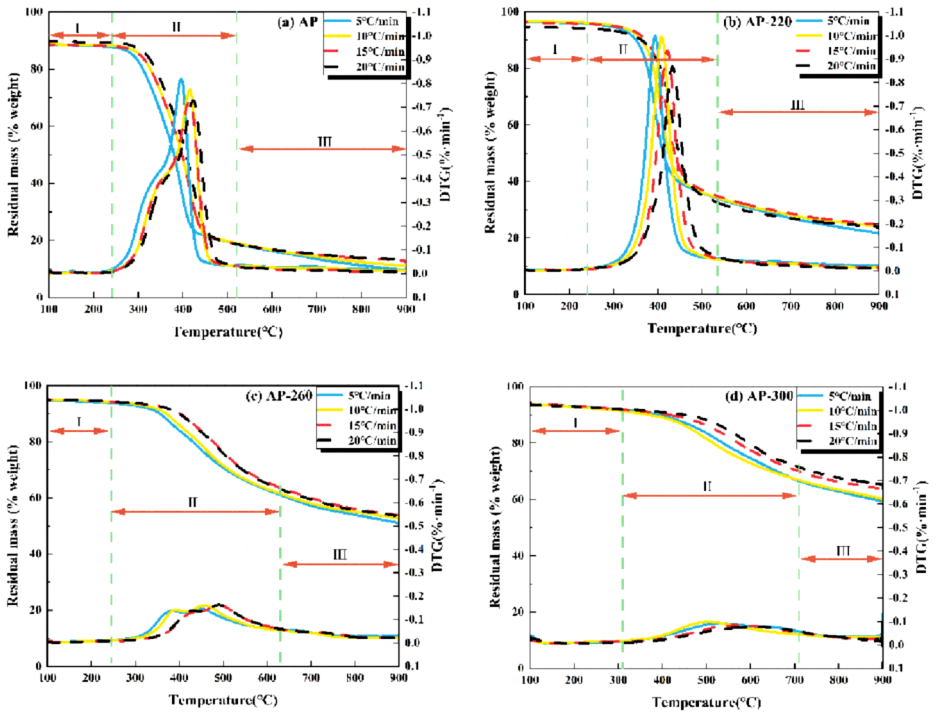

Figure 3. TG and DTG analyses of raw biomass and torrefied biomass at different heating rates: (a) AP, (b) AP-220, (c) AP-260, and (d) AP-300.

makes it appropriate for thermochemical conversion.[36] Furthermore, it may be cofired with other biomass or coal. The collision frequency of reactant molecules converting to products is represented by the pre-exponential factor *A*, and the average values of *A* for raw AP and torrefied AP estimated by the FWO, KAS, and DAEM models are shown in Table3. The values for raw AP are 1.34×10^{14}, 9.86×10^{13}, and 6.05×10^{13}; for AP-220, they are 5.11×10^{12}, 3.22×10^{12}, and 1.51×10^{12}; for AP-260, they are 3.17×10^{07}, 7.41×10^{06}, and 3.46×10^{06}, and for AP-300 they are 7.83×10^{04}, 7.77×10^{03}, and 9.15×10^{03}. It is observed that the pre-exponential factor decreases as the torrefaction temperature increases. A low pre-exponential component suggests a slower pace of reaction and necessitates a longer reaction time. Conversely, a large pre-exponential factor denotes a higher rate of reaction and allows for a quicker pace of reaction.[24,50] The variation of the pre-exponential factor could be attributed to the complexity of biomass as well as the complexity of biomass pyrolysis.

Estimating kinetic parameters is extremely important for the efficient design and scaling-up of industrial-scale reactors. For the kinetic study of raw materials and torrefied biomass, the Flynn−Wall−Ozawa (FWO), Kissinger−Akahira−Sunose (KAS), and distributed activation energy model (DAEM) models were used, with conversion rates ranging from 0.3 to 0.7. Figure 4 depicts the acquired isoconversional plots for raw materials and torrefied biomass (AP-220, AP-260, and AP-300). The slopes of the isoconversional lines, which are used to calculate the activation energy, alter as the conversion rate increases. As a result, the activation energy's value fluctuates. The activation energy, as given in the table, is comparable to the fluctuation in conversion rate represented in the graph. The activation energy derived from the FWO, KAS, and DAEM techniques is equivalent for both raw and torrefied biomasses (AP-220, AP-260, and AP-300). The activation energy obtained by the FWO model is somewhat greater than those calculated by the KAS and DAEM models, as indicated in the table. The variation in activation energy across models can be traced to the assumptions utilized in each technique. The fluctuation in activation energy with conversion throughout the pyrolysis process implies that the biomass conversion process is multistep and complicated, rather than single-step. As a result, the overall breakdown of biomass is established via a multistep response mechanism, with each stage contributing to the global mechanism in part dependent on the degree of decomposition.[36]

3.4. Prediction of Reaction Mechanisms. As shown in Figure 5, the prediction of the pyrolysis reaction model for raw biomass and torrefied biomass (AP-220, AP-260, and AP-300) under heating conditions at a rate of 10 °C/min was performed using the main function plot method combined with the Criado method. The pyrolysis mechanisms of raw AP and torrefied AP are most similar to theoretical curves D1, D2, D3, and D4, which correspond to one-dimensional diffusion models, two-dimensional diffusion models (Valensi models), and three-dimensional diffusion models (Jander models and Ginstlinge−Brounshtein models), respectively. AP-260 follows the R2 model, which corresponds to second-order random nucleation with two nuclei on a single particle (R2), while AP-300 follows the R2 and R3 models, which correspond to second-order random nucleation with two nuclei on a single particle (R2) and third-order random nucleation with three nuclei on a single particle (R3), respectively. The diffusion models AP and AP-220 have a larger volatile content, as seen in Table 1. On the contrary, the volatile compounds in AP-260 and AP-300 have already been released during the torrefaction process as the torrefaction temperature rises. As a result, the random nucleation model takes center stage. These findings are congruent with those of Doddapaneni et al.[33] and Mishra et al.[38] When the conversion rate exceeds 0.5, the raw biomass approaches theoretical curve R2, which corresponds to second-order random nucleation with two nuclei on a single particle, as well as the Avrami−Erofeev model (A1, A2, A3, and A4)

https://doi.org/10.1021/acsomega.3c07179
ACS Omega 2024, 9, 4474−4485

Table 3. Kinetic Parameters of AP Before and After Torrefaction

		FWO			KAS			DAEM		
	α	E (kJ/mol)	A (min^{-1})	R^2	E (kJ/mol)	A (min^{-1})	R^2	E (kJ/mol)	A min^{-1}	R^2
AP	0.3	148.66	1.19×10^{12}	0.9857	146.32	6.68×10^{11}	0.9838	146.32	1.02×10^{12}	0.9838
	0.4	168.15	2.76×10^{13}	0.9889	166.48	1.86×10^{13}	0.9875	166.48	1.98×10^{13}	0.9875
	0.5	181.13	1.71×10^{14}	0.9902	179.83	1.27×10^{14}	0.9891	179.83	9.97×10^{13}	0.9891
	0.6	185.52	2.37×10^{14}	0.9904	184.21	1.77×10^{14}	0.9893	184.21	1.05×10^{14}	0.9893
	0.7	187.18	2.32×10^{14}	0.9908	185.77	1.70×10^{14}	0.9897	185.77	7.69×10^{13}	0.9897
	average	174.13	1.34×10^{14}	0.9892	172.52	9.86×10^{13}	0.9879	172.52	6.05×10^{13}	0.9879
AP-220	0.3	177.9	3.41×10^{11}	0.9995	174.97	1.76×10^{11}	0.9994	174.97	2.69×10^{11}	0.9994
	0.4	171.13	9.63×10^{10}	0.9958	167.67	4.40×10^{10}	0.9950	167.67	4.69×10^{10}	0.9950
	0.5	171.09	9.39×10^{10}	0.9916	167.50	4.18×10^{10}	0.9901	167.50	3.28×10^{10}	0.9901
	0.6	176.79	2.36×10^{11}	0.9858	173.34	1.10×10^{11}	0.9835	173.34	6.57×10^{10}	0.9835
	0.7	205.33	2.48×10^{13}	0.9777	203.14	1.57×10^{13}	0.9747	203.14	7.12×10^{12}	0.9747
	average	180.45	5.11×10^{12}	0.9901	177.324	3.22×10^{12}	0.9885	177.324	1.51×10^{12}	0.9885
AP-260	0.3	67.95	3.25×10^{04}	0.9925	60.36	2.81×10^{03}	0.9900	60.36	4.29×10^{03}	0.9900
	0.4	77.31	1.12×10^{05}	0.9931	69.58	1.15×10^{04}	0.9909	69.58	1.22×10^{04}	0.9909
	0.5	97.04	1.89×10^{06}	0.9890	89.76	2.83×10^{05}	0.9857	89.76	2.22×10^{05}	0.9857
	0.6	113.88	1.60×10^{07}	0.9952	106.91	3.06×10^{06}	0.9940	106.91	1.82×10^{06}	0.9940
	0.7	134.34	1.41×10^{08}	0.9999	127.64	3.37×10^{07}	0.9999	127.64	1.52×10^{07}	0.9999
	average	98.10	3.17×10^{07}	0.9939	90.85	7.41×10^{06}	0.9921	90.85	3.46×10^{06}	0.9921
AP-300	0.3	78.51	1.34×10^{05}	0.9874	75.75	1.33×10^{04}	0.9838	75.75	2.04×10^{04}	0.9838
	0.4	84.04	1.93×10^{05}	0.9840	77.14	1.92×10^{04}	0.9875	77.14	2.05×10^{04}	0.9875
	0.5	85.61	6.09×10^{04}	0.9899	79.83	5.93×10^{03}	0.9891	79.83	4.66×10^{03}	0.9891
	0.6	86.28	3.89×10^{03}	0.9862	82.41	3.60×10^{02}	0.9893	82.41	2.14×10^{02}	0.9893
	0.7	88.92	3.12×10^{02}	0.9825	91.08	2.95×10^{01}	0.9897	91.08	1.34×10^{01}	0.9897
	average	84.67	7.83×10^{04}	0.9860	81.24	7.77×10^{03}	0.9879	81.24	9.15×10^{03}	0.9879

https://doi.org/10.1021/acsomega.3c07179
ACS Omega 2024, 9, 4474−4485

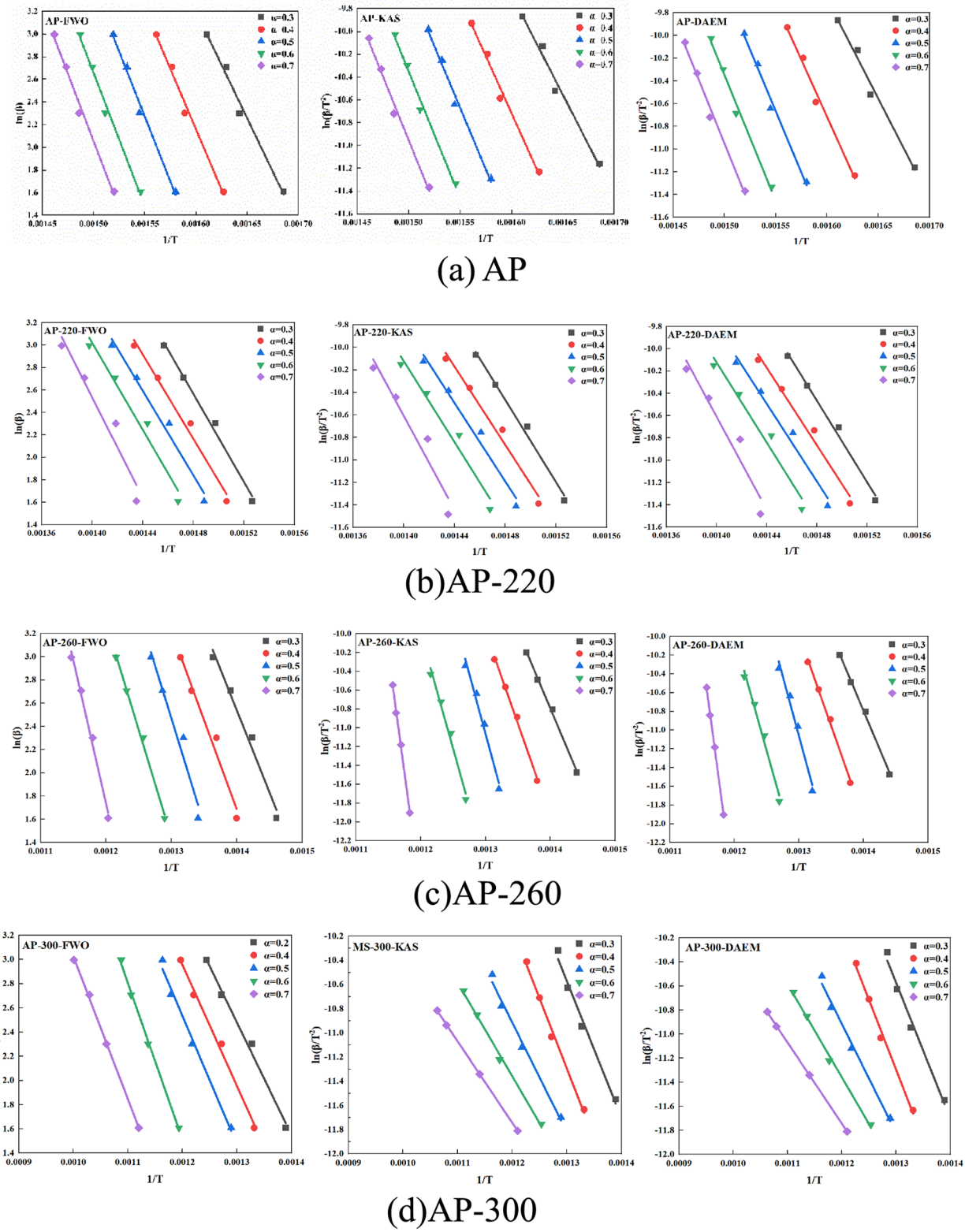

Figure 4. Thermal breakdown kinetics of AP before and after torrefaction were evaluated using the FWO, KAS, and DAEM techniques. AP (a), AP-220 (b), AP-260 (c), and AP-300 (d).

associated with nucleation and growth. AP-220, on the other hand, adheres to the R2 model, which corresponds to third-order random nucleation with two nuclei on a single particle (R2). It seems that the temperature has a certain impact on the conversion rate. Some ordered cellulose may depolymerize at higher temperatures, turning it into smaller molecular weight chains.[36] These smaller molecular weight chains might be used as locations for random nucleation, growth, and degradation processes.

3.5. Thermodynamic Parameters. The thermodynamic parameters, including Gibbs free energy (ΔG), enthalpy change (ΔH), and entropy change (ΔS), obtained from the

https://doi.org/10.1021/acsomega.3c07179
ACS Omega 2024, 9, 4474−4485

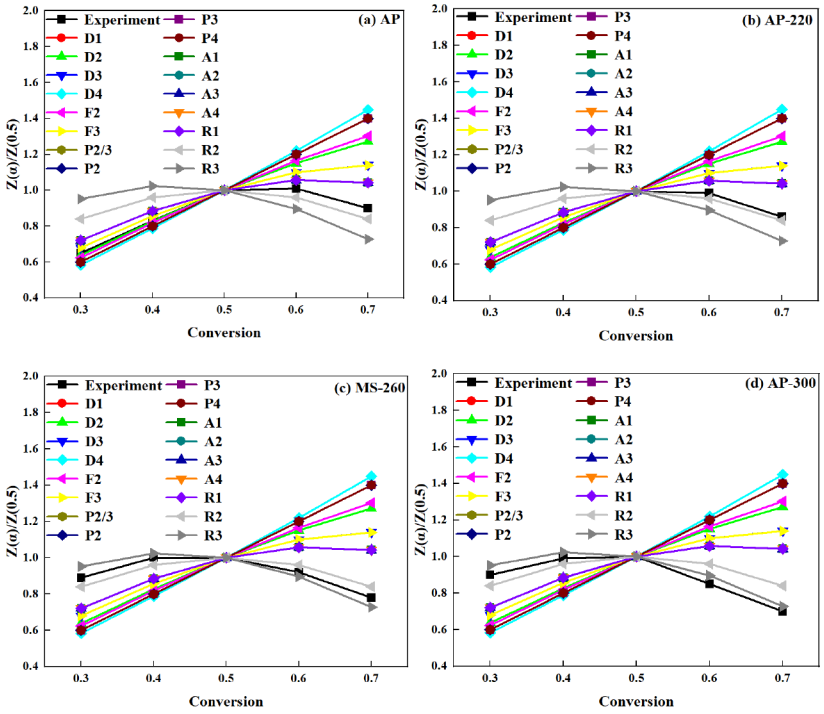

Figure 5. The theoretical and experimental plots (Z-master plot) of solid reaction mechanisms predicted by using the Criado method for (a) AP, (b) AP-220, (c) AP-260, and (d) AP-300.

Table 4. FWO, KAS, and DAEM Methods Were Used to Calculate the Thermodynamic Parameters of Raw AP and Torrefied AP

		FWO			KAS			DAEM		
	α	ΔG (kJ/mol)	ΔH (kJ/mol)	ΔS (kJ/mol)	ΔG (kJ/mol)	ΔH (kJ/mol)	ΔS (kJ/mol)	ΔG (kJ/mol)	ΔH (kJ/mol)	ΔS (kJ/mol)
AP	0.3	148.68	143.73	−8.34	148.68	141.39	−12.30	148.68	141.39	−12.30
	0.4	154.21	163.04	14.37	154.21	161.37	11.65	154.21	161.37	11.65
	0.5	158.94	175.87	26.75	158.94	174.57	24.69	158.94	174.57	24.69
	0.6	162.58	180.14	27.15	162.58	178.84	25.14	162.58	178.84	25.14
	0.7	165.43	181.71	24.75	165.43	180.30	22.60	165.43	180.30	22.60
	average	157.97	168.90	16.93	157.97	167.29	14.36	157.97	167.29	14.36
AP-220	0.3	164.71	152.46	−18.71	164.71	149.53	−23.19	164.71	149.53	−23.19
	0.4	167.01	145.61	−32.23	167.01	142.15	−37.44	167.01	142.15	−37.44
	0.5	169.07	145.50	−35.07	169.07	141.91	−40.42	169.07	141.91	−40.42
	0.6	171.52	151.12	−29.93	171.52	147.67	−35.00	171.52	147.67	−35.00
	0.7	175.59	179.54	5.66	175.59	177.35	2.52	175.59	177.35	2.52
	average	169.58	154.85	−22.06	169.58	151.72	−26.71	169.58	151.72	−26.71
AP-260	0.3	159.87	62.66	−152.75	159.87	55.07	−164.68	159.87	55.07	−164.68
	0.4	169.59	71.70	−145.27	169.59	63.98	−156.73	169.59	63.98	−156.73
	0.5	179.72	91.12	−124.31	179.72	83.83	−134.53	179.72	83.83	−134.53
	0.6	189.06	107.66	−108.74	189.06	100.69	−118.06	189.06	100.69	−118.05
	0.7	201.70	127.72	−92.83	201.70	121.02	−101.24	201.70	121.02	−101.24
	average	179.99	92.17	−124.78	179.99	84.92	−135.05	179.99	84.92	−135.05
AP-300	0.3	181.54	72.52	−151.47	181.54	69.76	−155.30	181.54	69.76	−155.30
	0.4	189.69	77.80	−148.99	189.69	70.90	−158.18	189.69	70.90	−158.18
	0.5	196.13	79.16	−150.80	196.13	73.38	−158.24	196.13	73.38	−158.24
	0.6	201.90	79.65	−153.25	201.90	75.78	−158.09	201.90	75.78	−158.09
	0.7	207.65	82.11	−153.14	207.65	84.26	−150.51	207.65	84.26	−150.51
	average	195.38	78.25	−151.53	195.38	74.82	−156.06	195.38	74.82	−156.06

process of torrefied AP along with their variations with conversion rate are shown in Table4. Thermodynamics studies the laws of energy exchange, and the thermodynamic properties of a system are state functions, which will help investigate the energy changes during the pyrolysis process.

Gibbs free energy (G) is the change in total energy increase of a system after the development of an activated complex.[24] Raw and torrefaction biomass Gibbs free energy values (AP-220, AP-260, and AP-300) are 148.68−165.43 kJ/mol, 164.71−175.29 kJ/mol, 159.87−201.70 kJ/mol, and 181.54−

https://doi.org/10.1021/acsomega.3c07179
ACS Omega 2024, 9, 4474−4485

207.65 kJ/mol, respectively. The fact that the Gibbs free energy is positive suggests that the biomass pyrolysis process is not spontaneous and requires external energy for thermal breakdown. The average value of ΔG for torrefied AP increases with the conversion rate, according to the three models. Positive ΔG values suggest that the raw and torrefaction biomasses (AP-220, AP-260, and AP-300) exhibit unfavorable processes that require substantial energy.[33] The increase in the Gibbs free energy of biomass after torrefaction is caused by chemical reactions and material transformations that occur during the torrefaction process. These chemical reactions involve the pyrolysis and other processes of organic molecules, resulting in the production of substantial volumes of gas and organic debris. These reactions demand energy, which increases the Gibbs free energy. Furthermore, heat loss and energy conversion occur throughout the torrefaction process, leading to a rise in the system's Gibbs free energy. As a result, the increase in Gibbs free energy of the biomass following torrefaction is the outcome of chemical processes and energy conversion.

Enthalpy is a thermodynamic property that represents the total heat content of a system. In the case of biomass pyrolysis, it signifies the total amount of heat absorbed when biomass is converted into different products, such as biochar, bio-oil, and gases. The average ΔH values, calculated using the FWO and KAS models, respectively, decreased from 168.90 to 78.25 kJ/mol and from 167.29 to 74.28 kJ/mol. The positive values of ΔH for biomass during the pyrolysis process indicate that the endothermic reactions dominate in parallel reactions. The cellulose content of AP-220 is slightly higher than that of AP, resulting in higher ΔH values compared to those of the raw biomass. During the torrefaction process, the moisture and volatile components in the biomass gradually evaporate and burn, leading to a reduction in its mass. Therefore, the enthalpy change (i.e., heat change) becomes lower. Specifically, the enthalpy change refers to the change in energy within a system at a certain temperature. The moisture and volatile components in biomass contain high energy, and when they are evaporated and burned, the energy within the system decreases, resulting in a decrease in enthalpy change.[51] Additionally, during the torrefaction process, the main components of biomass, such as cellulose and lignin, undergo chemical structural changes, which also contribute to a decrease in the enthalpy change. In conclusion, the enthalpy change of biomass after torrefaction becomes lower due to the loss of moisture and volatile components and the chemical structural changes that lead to a decrease in the energy within the system.

Entropy is a state function that represents the level of disorder or unpredictability in a response system.[52] The results show that the average ΔS values computed using the FWO and KAS models declined from 16.93 to −151.53 kJ/mol and from 14.36 to −156.06 kJ/mol, respectively. Larger ΔS values indicate that the biomass samples are distant from thermodynamic equilibrium, whereas decreasing ΔS values indicate that the biomass samples are gaining a new state that is near thermodynamic equilibrium. However, the ΔS values for AP-260 and AP-300 are negative, suggesting that the products generated via bond dissociation are disordered. The low entropy values also suggest that the components have recently experienced certain physical and chemical changes, allowing them to enter a thermodynamic equilibrium state during the pyrolysis process. After torrefaction, the entropy change of biomass flips from positive to negative values, progressively diminishing. This is because organic substances undergo processes such as heat breakdown, oxidation, and dehydration during the torrefaction process, resulting in a more organized and stable structure. These reactions induce high-energy bonds in organic molecules to break, resulting in the creation of lower-energy products and a decrease in the system entropy. This phenomenon suggests that organic molecules undergo structural changes during torrefaction, making them more organized and stable. Organic components' moisture and volatile chemicals of organic components evaporate or degrade, while the remaining organic matter becomes more compact and stable. Torrefaction biomass becomes drier and tougher as a result of this. Furthermore, the torrefaction process may generate organic gas and smoke with a high organic component content, lowering the concentration of organic matter in the system and thereby decreasing entropy. In summary, the change in biomass entropy from positive to negative during torrefaction may be linked to structural changes in organic molecules, a decrease in the organic matter concentration, and a decrease in the system entropy.

4. CONCLUSION

This article studies the pyrolysis kinetics and thermodynamic parameters of sawdust biomass during the torrefaction process, indicating that sawdust has sufficient thermochemical conversion characteristics to bioenergy and also confirms that biomass can be used as a potential energy production raw material. The following conclusions are drawn:

Physical and chemical investigation reveals that the fixed carbon content of the torrefied biomass grew from 14.88% to 67.97% when compared to the original biomass. This is because water in the biomass evaporated and internal components continued to decompose owing to torrefaction. The H/C ratio drops by 0.69, the O/C ratio lowers by 0.62, and the calorific value increases from 17.98 MJ/kg to 32.47 MJ/kg as the temperature rises from 220 to 300 °C, progressively approaching the characteristics of combustible coal. Every attribute has been enhanced in comparison to the initial biomass.

The results of the fiber composition study indicate that the torrefaction biomass (AP-220) has a little greater cellulose content than the original biomass, and that the fiber content decreases with increasing temperature. The activation energy of AP-220 is larger than that of the original biomass due to the increased cellulose content. The average activation energy of AP-300 was determined to be 89.46 kJ/mol and 91.28 kJ/mol lower than that of the original biomass, respectively, under the FWO and KAS models. Enthalpy and activation energy differ slightly, which promotes the creation of activated complexes.

According to the principal function graph method. Thermodynamic research revealed that the torrefaction temperature had no effect on the average Gibbs free energy of AP, although there is a significant upward trend from 157.97 kJ/mol to 195.38 kJ/mol, the increase is not significant. The enthalpy changes of the FWO and KAS models decreased from 168.90 kJ/mol to 78.25 kJ/mol and 167.29 kJ/mol to 74.82 kJ/mol, respectively, while the entropy changes decreased from 16.93 kJ/mol

https://doi.org/10.1021/acsomega.3c07179
ACS Omega 2024, 9, 4474−4485

to −151.53 kJ/mol and 14.36 kJ/mol to −156.06 kJ/mol, indicating higher stability of the end products. It is noticed that at lower conversion value ($\alpha \leq 0.5$), the diffusion mechanism was rate determining for raw and AP-220; however, for AP-260 and AP-300, the second-order random nucleation model is dominant for rate determination. At higher conversion ($\alpha \geq 0.5$), raw and AP-220 follow the second order random nucleation and Avrami−Erofeev models, while, in case of AP-260 and AP-300, third-order random nucleation is dominant.

AUTHOR INFORMATION

Corresponding Authors

Yintao Song − *National-Local Joint Engineering Research Center of Biomass Refining and High-Quality Utilization, Changzhou Key Laboratory of Biomass Green, Safe & High Value Utilization Technology, Institute of Urban and Rural Mining, Changzhou Key Laboratory of Biomass Green, Safe & High Value Utilization Technology, Changzhou University, Changzhou 213164, China;* orcid.org/0009-0000-0847-4815; Email: S21020856152@smail.cczu.edu.cn

Peng Liu − *National-Local Joint Engineering Research Center of Biomass Refining and High-Quality Utilization, Changzhou Key Laboratory of Biomass Green, Safe & High Value Utilization Technology, Institute of Urban and Rural Mining, Changzhou Key Laboratory of Biomass Green, Safe & High Value Utilization Technology, Changzhou University, Changzhou 213164, China;* orcid.org/0000-0003-2418-5030; Email: liupeng@cczu.edu.cn

Authors

Ailing Lu − *Shangtian Environmental Restoration Co., Ltd, Changzhou 213164, China*

Dianer Wang − *Shangtian Environmental Restoration Co., Ltd, Changzhou 213164, China*

Guangdong Liao − *Shangtian Environmental Restoration Co., Ltd, Changzhou 213164, China*

Binguo Zheng − *School of Civil Engineering and Architecture, Zhengzhou Institute of Aviation Industry Management, Zhengzhou, Henan 450046, China*

Tingzhou Lei − *National-Local Joint Engineering Research Center of Biomass Refining and High-Quality Utilization, Changzhou Key Laboratory of Biomass Green, Safe & High Value Utilization Technology, Institute of Urban and Rural Mining, Changzhou Key Laboratory of Biomass Green, Safe & High Value Utilization Technology, Changzhou University, Changzhou 213164, China*

Complete contact information is available at: https://pubs.acs.org/10.1021/acsomega.3c07179

Notes

The authors declare no competing financial interest.

ACKNOWLEDGMENTS

This study was funded by National Key R&D Program of China (2022YFB4201901), Natural Science Foundation of China (52306223 and 52306224), and Changzhou Sci & Tech Program (Grant nos. CE20222034, CJ20220246, and CJ20220138).

REFERENCES

(1) Jiang, B.; Xia, D. Toward carbon neutrality in China: A national wide carbon flow tracing and the CO_2 emission control strategies for CO_2-intensive industries. *Sci. Total Environ.* **2023**, *879*, 163009.

(2) Raza, T.; Shehzad, M.; Abbas, M.; Eash, N. S.; Jatav, H. S.; Sillanpaa, M.; Flynn, T. Impact assessment of COVID-19 global pandemic on water, environment, and humans. *Environ. Adv.* **2023**, 100328.

(3) Zhao, G.; Tian, S.; Wang, Y.; Liang, R.; Li, K. Quantitative assessment methodology framework of the impact of global climate change on the aquatic habitat of warm-water fish species in rivers. *Sci. Total Environ.* **2023**, *875*, 162686.

(4) Eekhout, J. P. C.; de Vente, J. Global impact of climate change on soil erosion and potential for adaptation through soil conservation. *Earth-Sci. Rev.* **2022**, *226*, 103921.

(5) Omar, M. E. D. M.; Moussa, A. M. A.; Hinkelmann, R. Impacts of climate change on water quantity, water salinity, food security, and socioeconomy in Egypt. *Water Sci. Eng.* **2021**, *14*, 17−27.

(6) Stowell, J. D.; Kim, Y.-M.; Gao, Y.; Fu, J. S.; Chang, H. H.; Liu, Y. The impact of climate change and emissions control on future ozone levels: Implications for human health. *Environ. Int.* **2017**, *108*, 41−50.

(7) Lu, S.; Bai, X.; Zhang, X.; Li, W.; Tang, Y. The impact of climate change on the sustainable development of regional economy. *J. Clean. Prod.* **2019**, *233*, 1387−1395.

(8) Ghoniem, A. F. Needs, resources and climate change: Clean and efficient conversion technologies. *Prog. Energy Combust. Sci.* **2011**, *37*, 15−51.

(9) Liu, X.; Liu, Z. Exploring the impact of media discourse on social perceptions towards biomass energy utilization in China. *Energy Strategy Rev.* **2022**, *42*, 100896.

(10) Kevser, M.; Tekbaş, M.; Doğan, M.; Koyluoglu, S. Nexus among biomass energy consumption, economic growth, and financial development: Evidence from selected 15 countries. *Energy Rep.* **2022**, *8*, 8372−8380.

(11) Sayed, E. T.; Wilberforce, T.; Elsaid, K.; Rabaia, M. K. H.; Abdelkareem, M. A.; Chae, K.-J.; Olabi, A. G. A critical review on environmental impacts of renewable energy systeAP and mitigation strategies: Wind, hydro, biomass and geothermal. *Sci. Total Environ.* **2021**, *766*, 144505.

(12) Cellura, M.; La Rocca, V.; Longo, S.; Mistretta, M. Energy and environmental impacts of energy related products (ErP): A case study of biomass-fuelled systeAP. *J. Clean. Prod.* **2014**, *85*, 359−370.

(13) Hussain, S. A.; Razi, F.; Hewage, K.; Sadiq, R. The perspective of energy poverty and 1st energy crisis of green transition. *Energy* **2023**, *275*, 127487.

(14) Shah, S. A. R.; Naqvi, S. A. A.; Riaz, S.; Anwar, S.; Abbas, N. Nexus of biomass energy, key determinants of economic development and environment: A fresh evidence from Asia. *Renewable and Sustainable Energy Rev.* **2020**, *133*, 110244.

(15) Vukašinović, V.; Gordić, D. Optimization and GIS-based combined approach for the determination of the most cost-effective investments in biomass sector. *Appl. Energy* **2016**, *178*, 250−259.

(16) Zhang, R.; Xu, G.; Li, B.; Wang, Z.; Gao, J.; Li, J.; Sun, Y.; Xu, G. Analysis of the pollution emission system of large-scale combustion of biomass briquette fuel in China. *Process Saf. Environ. Prot.* **2023**, *169*, 928−936.

(17) Sun, Y.; Wang, S.; Yang, Q.; Li, J.; Wang, L.; Zhang, S.; Yang, H.; Chen, H. Environmental impact assessment of VOC emissions from biomass gasification power generation system based on life cycle analysis. *Fuel* **2023**, *335*, 126905.

(18) Ji, L.; Zheng, Z.; Huang, Y.; Xie, Y.; Sun, L.; Huang, G. An integrated decision support method for strategic planning and tactical management of regional biomass power plants under uncertainties. *J. Clean. Prod.* **2023**, *388*, 135968.

(19) Li, J.; Gan, C.; Zhou, J.; Novakovic, V. Performance analysis of biomass direct combustion heating and centralized biogas supply system for rural districts in China. *Energy Convers. Manage.* **2023**, *278*, 116730.

(20) Qiu, B.; Tao, X.; Wang, J.; Liu, Y.; Li, S.; Chu, H. Research progress in the preparation of high-quality liquid fuels and chemicals by catalytic pyrolysis of biomass: A review. *Energy Convers. Manage.* **2022**, *261*, 115647.
(21) Gin, A. W.; Hassan, H.; Ahmad, M. A.; Hameed, B. H.; Mohd Din, A. T. Recent progress on catalytic co-pyrolysis of plastic waste and lignocellulosic biomass to liquid fuel: The influence of technical and reaction kinetic parameters. *Arab. J. Chem.* **2021**, *14*, 103035.
(22) Uslu, A.; Faaij, A. P. C.; Bergman, P. C. A. Pre-treatment technologies, and their effect on international bioenergy supply chain logistics. Techno-economic evaluation of torrefaction, fast pyrolysis and pelletisation. *Energy* **2008**, *33*, 1206−1223.
(23) Sriram, A.; Swaminathan, G. Pyrolysis of Musa balbisiana flower petal using thermogravimetric studies. *Bioresour. Technol.* **2018**, *265*, 236−246.
(24) Kaur, R.; Gera, P.; Jha, M. K.; Bhaskar, T. Pyrolysis kinetics and thermodynamic parameters of castor (*Ricinus communis*) residue using thermogravimetric analysis. *Bioresour. Technol.* **2018**, *250*, 422−428.
(25) Mallick, D.; Poddar, M. K.; Mahanta, P.; Moholkar, V. S. Discernment of synergism in pyrolysis of biomass blends using thermogravimetric analysis. *Bioresour. Technol.* **2018**, *261*, 294−305.
(26) Wu, Z.; Yang, W.; Tian, X.; Yang, B. Synergistic effects from co-pyrolysis of low-rank coal and model components of microalgae biomass. *Energy Convers. Manage.* **2017**, *135*, 212−225.
(27) Meng, H.; Wang, S.; Wu, Z.; Zhao, J.; Chen, L.; Li, J. Thermochemical behavior and kinetic analysis during co-pyrolysis of starch biomass model compound and lignite. *Energy Procedia* **2019**, *158*, 400−405.
(28) Yang, F.; Zhou, A.; Zhao, W.; Yang, Z.; Li, H. Thermochemical behaviors, kinetics and gas emission analyses during co-pyrolysis of walnut shell and coal. *Thermochim. Acta* **2019**, *673*, 26−33.
(29) Bach, Q.-V.; Trinh, T. N.; Tran, K.-Q.; Thi, N. B. D. Pyrolysis characteristics and kinetics of biomass torrefied in various atmospheres. *Energy Convers. Manage.* **2017**, *141*, 72−78.
(30) Zhang, S.; Dong, Q.; Zhang, L.; Xiong, Y. Effects of water washing and torrefaction on the pyrolysis behavior and kinetics of rice husk through TGA and Py-GC/AP. *Bioresour. Technol.* **2016**, *199*, 352−361.
(31) Hu, Q.; Yang, H.; Xu, H.; Wu, Z.; Lim, C. J.; Bi, X. T.; Chen, H. Thermal behavior and reaction kinetics analysis of pyrolysis and subsequent in-situ gasification of torrefied biomass pellets. *Energy Convers. Manage.* **2018**, *161*, 205−214.
(32) Castells, B.; Amez, I.; Medic, L.; García-Torrent, J. Torrefaction influence on combustion kinetics of Malaysian oil palm wastes. *Fuel Process. Technol.* **2021**, *218*, 106843.
(33) Doddapaneni, T. R. K. C.; Konttinen, J.; Hukka, T. I.; Moilanen, A. Influence of torrefaction pretreatment on the pyrolysis of Eucalyptus clone: A study on kinetics, reaction mechanism and heat flow. *Ind. Crop. Prod.* **2016**, *92*, 244−254.
(34) Bach, Q.-V.; Tran, K.-Q.; Skreiberg, Ø. Comparative study on the thermal degradation of dry- and wet-torrefied woods. *Appl. Energy* **2017**, *185*, 1051−1058.
(35) Peltre, C.; Dignac, M. F.; Derenne, S.; Houot, S. Change of the chemical composition and biodegradability of the Van Soest soluble fraction during composting: A study using a novel extraction method. *Waste Manage.* **2010**, *30*, 2448−2460.
(36) Singh, S.; Prasad Chakraborty, J.; Mondal, M. K. Intrinsic kinetics, thermodynamic parameters and reaction mechanism of non-isothermal degradation of torrefied *Acacia nilotica* using isoconversional methods. *Fuel* **2020**, *259*, 116263.
(37) Dhyani, V.; Kumar, J.; Bhaskar, T. Thermal decomposition kinetics of sorghum straw via thermogravimetric analysis. *Bioresour. Technol.* **2017**, *245*, 1122−1129.
(38) Mishra, G.; Kumar, J.; Bhaskar, T. Kinetic studies on the pyrolysis of pinewood. *Bioresour. Technol.* **2015**, *182*, 282−288.
(39) Yang, Y.; Qu, X.; Huang, G.; Ren, S.; Dong, L.; Sun, T.; Liu, P.; Li, Y.; Lei, T.; Cai, J. Insight into lignocellulosic biomass torrefaction kinetics with case study of pinewood sawdust torrefaction. *Renewable Energy* **2023**, *215*, 118941.
(40) Odiyi, D. C.; Sharif, T.; Choudhry, R. S.; Mallik, S. Cure mechanism and kinetic prediction of biobased glass/polyfurfuryl alcohol prepreg by model-free kinetics. *Thermochim. Acta* **2022**, *708*, 179133.
(41) Lim, A. C. R.; Chin, B. L. F.; Jawad, Z. A.; Hii, K. L. Kinetic Analysis of Rice Husk Pyrolysis Using Kissinger-Akahira-Sunose (KAS) Method. *Procedia Eng.* **2016**, *148*, 1247−1251.
(42) Chen, D.; Gao, A.; Ma, Z.; Fei, D.; Chang, Y.; Shen, C. In-depth study of rice husk torrefaction: Characterization of solid, liquid and gaseous products, oxygen migration and energy yield. *Bioresour. Technol.* **2018**, *253*, 148−153.
(43) Chen, W.-H.; Liu, S.-H.; Juang, T.-T.; Tsai, C.-M.; Zhuang, Y.-Q. Characterization of solid and liquid products from bamboo torrefaction. *Appl. Energy* **2015**, *160*, 829−835.
(44) Saikia, R.; Baruah, B.; Kalita, D.; Pant, K. K.; Gogoi, N.; Kataki, R. Pyrolysis and kinetic analyses of a perennial grass (*Saccharum ravannae L.*) from north-east India: Optimization through response surface methodology and product characterization. *Bioresour. Technol.* **2018**, *253*, 304−314.
(45) Ren, S.; Lei, H.; Wang, L.; Bu, Q.; Chen, S.; Wu, J. Thermal behaviour and kinetic study for woody biomass torrefaction and torrefied biomass pyrolysis by TGA. *Biosyst. Eng.* **2013**, *116*, 420−426.
(46) Yang, H.; Yan, R.; Chen, H.; Lee, D. H.; Zheng, C. Characteristics of hemicellulose, cellulose and lignin pyrolysis. *Fuel* **2007**, *86*, 1781−1788.
(47) Zhao, B.; Yang, H.; Zhang, H.; Zhong, C.; Wang, J.; Zhu, D.; Guan, H.; Sun, L.; Yang, S.; Chen, L. Study on hydrogen-rich gas production by biomass catalytic pyrolysis assisted with magnetic field. *J. Anal. Appl. Pyrolysis* **2021**, *157*, 105227.
(48) Cardarelli, A.; Pinzi, S.; Barbanera, M. Effect of torrefaction temperature on spent coffee grounds thermal behaviour and kinetics. *Renew. Energy* **2022**, *185*, 704−716.
(49) Vamvuka, D.; Kakaras, E.; Kastanaki, E.; Grammelis, P. Pyrolysis characteristics and kinetics of biomass residuals mixtures with lignite☆. *Fuel* **2003**, *82*, 1949−1960.
(50) Yuan, X.; He, T.; Cao, H.; Yuan, Q. Cattle manure pyrolysis process: Kinetic and thermodynamic analysis with isoconversional methods. *Renewable Energy* **2017**, *107*, 489−496.
(51) Merdun, H.; Laougé, Z. B. Kinetic and thermodynamic analyses during co-pyrolysis of greenhouse wastes and coal by TGA. *Renewable Energy* **2021**, *163*, 453−464.
(52) Sinha, D. Entropy changes in a thermodynamic process under potential gradients. *Phys. A* **2014**, *416*, 676−683.

https://doi.org/10.1021/acsomega.3c07179
ACS Omega 2024, 9, 4474−4485